METANE
An Integrated Project to
Model undErwater gas/oil blowouT And lNg lEak

Hellouvry Yann-Hervé [1], Parthenay Valérie [1],
Aprin Laurent [2], Le Floch Stéphane [3], Van Ganse Sophie [3],
Blanchetière Gaël [4], Mouriès Magali [5]

(1) Alyotech Technologies, Rennes, France
(2) LGEI, Ecole des Mines d'Alès, Alès, France
(3) CEDRE, Brest, France
(4) GDF SUEZ, Paris, France
(5) Nymphéa Environnement, Cassis, France
valerie.parthenay@alyotech.fr

Abstract

During the last decades, several dramatic accidents have occurred on Oil & Gas platforms. To date, the accident involving the Deepwater Horizon platform in the Gulf of Mexico in April 2010 was the most catastrophic accident in the world, in which 11 people died and an estimated 4.9 million barrels of oil was released from the well. These accidents, their potential consequences and impacts (toxic pollution, explosion and fire) confirm the relevance of investigations into these submarine phenomena. The METANE project addresses the operational challenges that involve better understanding of the complexity of accidental subsea releases with a decision-support system able to help in the mitigation of safety-related and ecological impacts. The METANE consortium covers all spheres: institutional, academic and private partners.

The main innovative part of the project consists in the characterization of oil and gas behaviour in a water column and their fate in the atmosphere. The gas part has been developed in the context of the CITEPH project 71-2011 "Underwater gas and LNG leaks" (see section 7).

This paper deals with the development of the gas blowout model based on the Lagrangian concept. The jet-plume mathematical model covers various constraints related to exploitation of fossil resources including LNG. This theoretical model includes physico-chemical processes at bubble scale and takes into account hydrate formation and decomposition, gas dissolution and bubble slip velocity. Results from this model were then compared with experimental data obtained at the *Ecole des Mines d'Alès* (EMA) to characterize the influence of pressure on the behaviour of oil and gas bubbles in the water column and with those obtained at CEDRE to determine the influence of breach characteristics on the oil and gas plume features. The model provides visualization of the underwater jet-plume trajectory depending on environmental conditions and on leak and release parameters with an estimation of pollutant mass flow rate, plume ascent time and concentration in the water column. In addition, a 3D visualization tool can be implemented in case of accident or for contingency planning.

The model estimates the impact of the gas leak at the sea surface allowing risk evaluation of buoyancy loss for the floating structures. For LNG or gas reaching the sea surface, this modelling could be also combined with atmospheric dispersion models to define the hazardous area due to the flammable gas cloud. The METANE project therefore proposes an integrated tool.

1.   Introduction

For many years, Oil & Gas industry stakeholders have clearly expressed their need for tools to predict and model oil and gas leaks. The accident involving the Deepwater Horizon platform in the Gulf of Mexico in April 2010 confirmed the importance of fully

understanding these underwater phenomena and their consequences at the sea surface. With this in mind, the purpose of the METANE project is to develop a decision-support tool for the implementation of contingency plans for industrial risks related to oil and gas leaks at sea, including LNG (Liquefied Natural Gas). The aim of this project is to improve both the safety of personnel on-board offshore Oil & Gas installations and the pollution response to limit the impact in the marine environment.

First this paper presents the jet-plume mathematical model based on a Lagrangian approach which takes account of both oil and gas, including for gas the hydrate formation/decomposition and dissolution in water. Experiments led by CEDRE and EMA on the influence of the injection flow rate, bubble slip velocity and pressure effect are then described. The next part presents the work realized by GDF SUEZ about coupling the results output for the gas part with atmospheric dispersion models. Finally, the METANE graphical user interface (GUI) is then detailed with some relevant screenshots.

2. Physical Model
4.1 Plume model

The oil release is treated in two different stages. An initial stage considers the part in which the hydrodynamics are governed by the plume mixing: the oil jet creates entrainment of the ambient water into the plume. Then the plume reaches a neutral buoyancy level (NBL), at which the dynamics of the plume end. In this case, the plume dynamics are no longer important and the passive advection and diffusion behaviour become the dominant process to transport the oil. The oil will rise as parcels of numerous droplets, following the ambient current and rising due to their own buoyancy.

The jet-plume part is based on a Lagrangian model (Lee and Cheung, 1990; Yapa and Zheng, 1997), in which a control volume is tracked as it moves along the centreline of the buoyant jet with its local centreline velocity $\mathbf{V}$ (m/s). The evolution of its properties, radius b (m), thickness $h = \mathbf{V}\Delta t$ (m), and mass $m = \rho\pi b^2 h$ (kg) is tracked over time. The mass variation in the plume is linked to the volume flux Q_e (m^3/s) oriented towards the inner structure and entrained by the turbulent eddies. The fluid in the control volume is considered as a mixture of water and oil forming a single phase with density ρ (kg/m^3). The conservation of the liquid mass m_l is:

$$\frac{dm_l}{dt} = \rho_a Q_e \qquad (1)$$

where ρ_a is the density of ambient water (kg/m^3). The volume flux Q_e is the result of the shear-induced entrainment between the buoyant jet and the water, and a forced entrainment due to the advection of current into the buoyant jet. Oil dissolution is neglected here.

The momentum equations are applied to the average within the control volume. The drag force is neglected. The momentum equations can be written as follows:

$$\frac{d}{dt}(m_l\mathbf{V}) = \mathbf{V}_a\rho_a Q_e + \mathbf{k}m_l\frac{(\rho_a - \rho_l)}{\rho_l}g \qquad (2)$$

where $\mathbf{V}_a$ is the velocity of the ambient environment (m/s) and a unit vector $\mathbf{k}$ in the vertical direction.

State variables like heat and salinity are also considered, following:

Parthenay, V., Y.-H. Hellouvry, A. Laurent, S. Le Floch, S. Van Ganse, G. Blanchetière and M. Mouriès, METANE: An Integrated Project to Model Underwater Gas/Oil Blowouts and LNG Leaks, Proceedings of the Thirty-seventh AMOP Technical Seminar on Environmental Contamination and Response, Environment Canada, Ottawa, ON, pp. 102-121, 2014.

$$\frac{d}{dt}[\, m_l C_{pl} T_{pl}\,] = C_{pa} T_a \rho_a Q_e \qquad\qquad (\,3\,)$$

$$\frac{d}{dt}[\, m_l S_{pl}\,] = S_a \rho_a Q_e \qquad\qquad (\,4\,)$$

where C_{pl} and C_{pa} are respectively the specific heat of the liquid in the control volume and specific heat of the ambient water (J/kg.K); T_{pl} and T_a respectively the temperature of the plume and of the ambient water (K); S_{pl} and S_a the salinity of the plume and of the ambient water (PSU).

4.2 Advection and Diffusion Model

As the plume moves upwards, it loses momentum and buoyancy due to entrainment of ambient water. The plume dynamics are no longer high. Then beyond this depth, the oil undergoes advection-diffusion combined with its own buoyant velocity. The pollutant is divided into a large number of Lagrangian parcels. At each time step, each particle is displaced according to the advective process (buoyancy, ambient current) with the velocity **U** and diffusive process (turbulent fluctuations). These particles are introduced at the end of the plume dynamics. Each particle displacement is as follows:

$$\frac{d\mathbf{X}}{dt} = \mathbf{U} + \mathbf{U}' \qquad\qquad (\,5\,)$$

where **X** is the position vector of the particle (m) and $\mathbf{U}'$ the diffusive velocity (m/s). The diffusion is modelled using a random walk algorithm. This fluctuating component of the current acting on particles is altered at each time step by a normal random deviation with amplitude specified by the root mean square of the fluctuating currents.

4.3 Slip Velocity

In plumes, there is a slip velocity w_s between rising fluid particles and the surrounding liquid within the plume area. In a droplet plume, it is the velocity difference between rising droplets and the surrounding water. The most used law to calculate this slip velocity is based on the Stokes' law but it approximates only small bubbles considered as perfect spheres. Clift et al. (1978) have shown that the shape of fluid particles could be approximated as a sphere for the small size range (smaller than 1 mm), an ellipsoid in the intermediate size range (1 mm to 15 mm), and a spherical-cap in the larger size range. They also demonstrated that shape has an important impact on the particle terminal velocity. For spherical bubbles the terminal velocity is influenced by the viscosity of the ambient fluid; for ellipsoidal bubbles the interfacial tension is the key factor, while neither the viscosity of the ambient fluid or interfacial tension influence spherical-cap bubbles.

Clift et al. (1978) offer several correlations for the different regimes of bubble shapes.
- The regime of spherical shape is given by:

$$w_s = \frac{\mu R_e}{\rho d} \qquad\qquad (\,6\,)$$

where R_e is the Reynolds number, μ the dynamic viscosity of ambient water (Pa.s), ρ the density of ambient fluid (kg/m^3) and d the spherical particle diameter (m).
- The regime of ellipsoidal shape is given by:

Parthenay, V., Y.-H. Hellouvry, A. Laurent, S. Le Floch, S. Van Ganse, G. Blanchetière and M. Mouriès, METANE: An Integrated Project to Model Underwater Gas/Oil Blowouts and LNG Leaks, Proceedings of the Thirty-seventh AMOP Technical Seminar on Environmental Contamination and Response, Environment Canada, Ottawa, ON, pp. 102-121, 2014.

$$w_s = \frac{\mu}{\rho d_e} M^{-0.149} (J - 0.857)$$ (7)

where d_e is the equivalent diameter (m), and:

$J = 0.94 H^{0.757}$ for $2 < H \le 59.3$

$J = 3.42 H^{0.441}$ for $H > 59.3$

H is defined as $H = \frac{4}{3} E_0 M^{-0.149} \left(\frac{\mu}{\mu_w} \right)^{-0.14}$ with μ_w the dynamic viscosity of water;

E_0 the Eötvös number defined as follows: $E_0 = \frac{g(\rho_l - \rho_g)d_e^2}{\sigma}$ with σ the interfacial

tension (N/m) and ρ_g the droplet/bubble density (kg/m³).

M the Morton number defined as follows: $M = \frac{g\mu^4 \Delta\rho}{\rho^2 \sigma^3}$

The criteria in this regime are M<10⁻³ and Eo<40.

- The regime of spherical-cap is given by:

$$w_s = 0.711 \sqrt{\frac{g d_e^2 (\rho_l - \rho_g)}{\rho_l}}$$ (8)

3. Integration of the BLOWOUT software

BLOWOUT is a software developed in the context of the CITEPH project 71-2011 "Underwater gas and LNG leaks" (see section 7). It focuses on natural gas releases including deep water behaviour such as dissolution and hydrate formation and decomposition, and LNG release for shallow water.

For natural gas releases, the plume model is also based on a Lagrangian model (Lee and Cheung, 1990; Yapa and Zheng, 1997). Additional terms have to be taken into account in momentum conservation equation (2) in order to consider the presence of gas:

$$\frac{d}{dt}((m_l + m_g)\mathbf{V} + \mathbf{k} w_s m_g) = \mathbf{V}_a \rho_a Q_e + \mathbf{V} \rho_g Q_g + ...$$
$$\mathbf{k}\left[(\rho_a - \rho_l)g\pi b^2 (1 - \beta\varepsilon h) - (\rho_a - \rho_g)g\pi b^2 \beta\varepsilon h\right]$$ (9)

where ρ_g and Q_g represent respectively the gas density (kg/m³) and the gas volume flux (m³/s), w_s here is the slip velocity of a gas bubble (m/s). ε is the void fraction of gas in the control volume such as $\varepsilon = \frac{\rho_l - \rho}{\rho_l - \rho_g}$. The continuous phase (liquid) and dispersed phase (bubbles) are treated as a single mixture with density ρ (kg/m³).

For the deep water, the assumption that the gas mass flow rate is constant at each cross section can no longer hold, and dissolution has to be taken into account: In a control volume, the dissolution rate is as follows:

$$\frac{dn_g}{dt} = KA(C_s - C_0)$$ (10)

Parthenay, V., Y.-H. Hellouvry, A. Laurent, S. Le Floch, S. Van Ganse, G. Blanchetière and M. Mouriès, METANE: An Integrated Project to Model Underwater Gas/Oil Blowouts and LNG Leaks, Proceedings of the Thirty-seventh AMOP Technical Seminar on Environmental Contamination and Response, Environment Canada, Ottawa, ON, pp. 102-121, 2014.

where n_g is the number of moles of gas in a bubble (mol), K is the mass transfer coefficient (m/s), A the surface area of the gas bubble (m^2), C_0 the concentration of the dissolved gas in ambient water (mol/m^3). K is computed depending on the bubble shape i.e. using different formulas for spherical, ellipsoidal and spherical cap shapes. (Clift et al., 1978). The saturated value or solubility is given by $Cs = x^l \dfrac{\rho_w}{M_w}$ (mol/m^3) with x^l the mole fraction of dissolved gas in water, ρ_w the water density (kg/m^3) and M_w the molecular weight of water (mol/kg).

Because of the limitation of Henry's law to low pressure or ideal gas, the solubility in water is calculated from a modified Henry's law based on the fugacity (Pa) as follows:

$$f_g = H \; x_l \; exp\left(\frac{Pv_l}{RT} \right) \qquad\qquad (\,11\,)$$

where P is the gas pressure (Pa), H the Henry's law constant (Pa), $R = 8.31\,(\mathrm{J/mol.K})$ the universal gas constant, T the water temperature (K) and v_l the partial molar volume of gas (m^3/mol).

The solubility of gas in water is strongly dependent on the ambient pressure, temperature and salinity. In deep water with high pressure, the ideal gas law breaks down. We have to consider the behaviour of a real gas, described as follows:

$$PV = ZnRT \qquad\qquad (\,12\,)$$

with Z the compressibility factor. The fugacity and the compressibility factor are calculated with the Peng-Robinson equation of state.

In deep water, pressures are very high and temperatures very low. This can affect gas bubbles, creating a hydrate shell around the bubble, and the plume can rise higher as dissolution is inhibited. Depending on the pressure-temperature couple relatively to a hydrate stability pressure-temperature curve, the hydrate can form or decompose. These phenomena are not well understood yet as they are complex processes. Based on Englezos et al. (1987) and Kim et al. (1986), kinetics, mass and heat transfer are taken into account for hydrate formation and decomposition, in order to calculate gas consumption rate in the plume.

LNG release has a different approach because of liquid/vapour phase transition. The aim here is to evaluate whether a LNG pool is formed or whether or not LNG vapour – which reaches the water surface –, is buoyant, with the risk of formation of a cold and heavy LNG cloud. The model is based on Raj and Bowdoin (2010) and considers the maximum size of liquid droplets formed by the jet (Okhotskii, 1988), their evaporation time, the distance of travel and the heating of the LNG vapour by the surrounding water until it reaches the surface. In a safety context, it is relevant to focus on the largest droplet because of its probable higher slip velocity and its slower heating.

From the breach, the liquid jet rises and breaks up: droplets are generated and scattered. Based on correlations, Okhotskii (1988) gives a formula for the maximum droplets regarding the mechanical forces acting on the breakup of the jet, i.e. jet instabilities but not thermal effects.

After the breakup of the jet, droplets rise and bubbles are formed, with the evaporation process. The rate of decrease of the droplet diameter due to evaporation is given by:

$$\frac{d\,V_d}{dt} = -\frac{h_{FB}A_d\left(T_W - T_{sat}\right)}{\lambda\rho_J} \tag{13}$$

where h_{FB} is a constant water-to-droplet film boiling heat transfer coefficient (W/m².K), A_d is the surface area of the droplet (m^2), V_d is the volume of the droplet (m^3), T_W and T_{sat} are respectively the water temperature, the temperature of saturation for the LNG estimated with the Clausius–Clapeyron relation (K), λ is the heat of vaporization of LNG (J/kg) and ρ_j is the jet density (kg/m^3).

Bubbles rise and warm up with the heating process. Bubble heating is linked to the convective heat flux depending on the temperature difference between the ambient water temperature and the gas bubble. The rate of heat transfer to the bubble from the ambient water is given by Newton's Law of cooling as follows:

$$\frac{dQ}{dt} = hA(T_w - T) \tag{14}$$

where Q is the thermal energy (J), h is the heat transfer coefficient (W/m².K), that we assume to be constant and A is the surface area of the bubble (m^2). Because of shallow water context, dissolution is neglected and the gas is assumed to have an ideal behaviour.

The correlations from Clift et al. (1978) are adopted here again in order to treat all the shape regimes of the droplets/bubbles. The effects of Rapid Phase Transition (RPT), potentially generating a large amount of energy and explosions (blast waves), are not considered.

4.   Experiments

Various studies have been performed to validate Clift's model and to characterize the motion of single bubbles or a chain of bubbles. The rise of a bubble in a liquid is assumed to be a one-dimensional approach along the vertical axis. The motion of a bubble is subjected to the buoyancy, drag force and the interfacial force (surface tension). Many studies deal with the influence of operating pressure on the bubble rise velocity in industrial processes and mainly for gas-liquid reactors (Wilkinson (1991), Luo et al. (1998)). It is well known that bubble size is controlled by hydrostatic pressure. Assuming the bubble is an ideal gas in an isothermal system, the bubble size increases during the rise through the liquid. This phenomenon is due to the decrease in the depth of liquid above the bubble which leads to a decrease in the static pressure.

Tests were performed at two different scales to analyse these phenomena. Atmospheric pressure tests were obtained from the CEDRE Experimental Column (CEC) and pressurised tests are performed in the pressurized column at the *Ecole des Mines d'Ales* in a range from 1 to 80 bar.

4.1   CEC Experiments

The CEDRE Experimental Column (CEC) (Figure 1) is equipped with an injection system, on which it is possible to set different nozzle diameters, and two high speed video recording systems. The CEC is a five meter high hexagonal column with a diameter of 1 m, and a total capacity of 4.50 m^3. The experimental design is described in the paper of Le Floch et al. (2009). To measure droplet velocity, two video cameras are used at different levels. The first camera is located 15 cm above the injection nozzle (4 m depth), at a pressure of 141325 Pa, and the second 15 cm below the surface (0.25 m depth), at a pressure of 102825 Pa. The distance between the 2 recording systems is 3.65 m. During the experiments, the temperature of the water is 284.15 K, with a salinity of 34 ppm.

Parthenay, V., Y.-H. Hellouvry, A. Laurent, S. Le Floch, S. Van Ganse, G. Blanchetière and M. Mouriès, METANE: An Integrated Project to Model Underwater Gas/Oil Blowouts and LNG Leaks, Proceedings of the Thirty-seventh AMOP Technical Seminar on Environmental Contamination and Response, Environment Canada, Ottawa, ON, pp. 102-121, 2014.
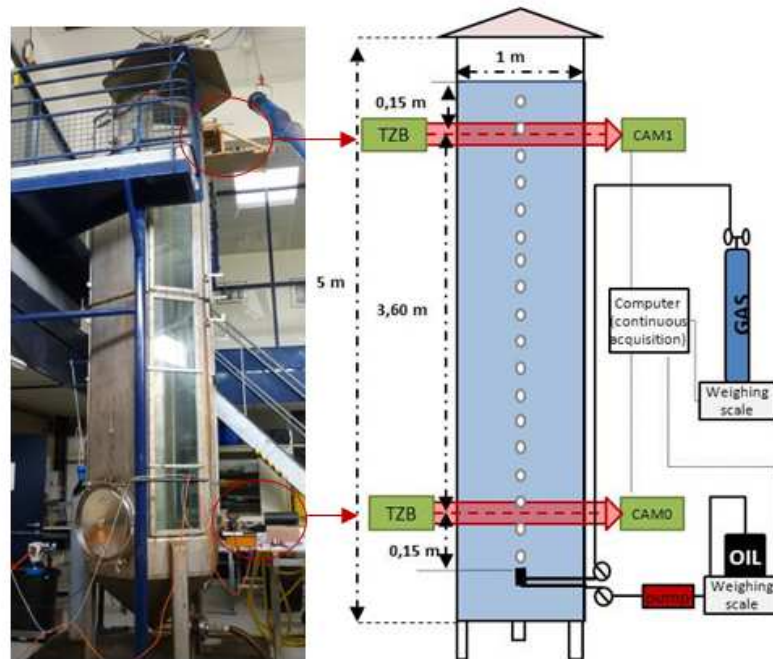
Figure 1. CEDRE Experimental Column designed with shadowgraphy equipment (2 lights and cameras on a parallel plane) and bubble injection system of gas or/and oil from the bottom (4 m depth).

Each sequence of images was processed to locate and track the bubble based on the detection of differences of gray level for each pixel on the images and thus isolate the bubble (dark) from the background (bright). The resulting binary images are introduced in Figure 2. This figure shows 8 images of the rise of a nitrogen bubble, whereby the time separating the first and the last picture is 109 milliseconds (ms). The time separating 2 images is 15.6 ms, and the position of the center of the bubble on the X and Y axes of the image allow the calculation of the bubble velocity (m.s^{-1}). The Waddel disk diameter, defined as the diameter of the disk with the same area as the particle, is used to calculate the gas volume and the dissolution kinetics.
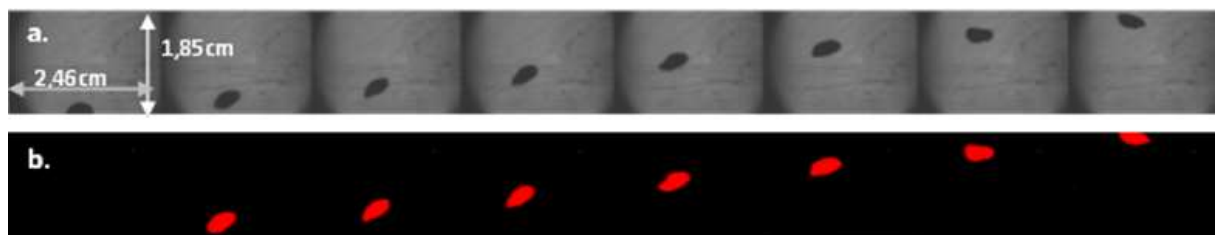
Figure 2. Pictures at 4 m depth with a flow rate of 0.5 µg/s with an injection nozzle of 1.5 mm. Ascension of a nitrogen bubble, with an acquisition rate of 64 image.s^{-1} by shadowgraph technique (a) and resulting binary images (b). The time interval between the first and the last image is 109 ms.

During the experiments, the bubbles had an oscillating spiral trajectory due to instabilities, which creates major uncertainties on bubble diameter. Figure 3 represents the bubble distribution at two different levels obtained for a nitrogen mass flow rate of 0.033 l/min and nozzle diameter of 4 mm. This figure clearly shows that all the bubble diameters are in a range between 4.5 mm to 6 mm. It indicates that there is a slightly difference between

Parthenay, V., Y.-H. Hellouvry, A. Laurent, S. Le Floch, S. Van Ganse, G. Blanchetière and M. Mouriès, METANE: An Integrated Project to Model Underwater Gas/Oil Blowouts and LNG Leaks, Proceedings of the Thirty-seventh AMOP Technical Seminar on Environmental Contamination and Response, Environment Canada, Ottawa, ON, pp. 102-121, 2014.

the bottom and the top of the column with a mean diameter of 49±1 mm at the bottom (4 m) and 53±3 mm at the top of the column. This difference is thought to be induced by the difference in pressure during the ascension and the oscillating trajectory of the bubble in the water column.
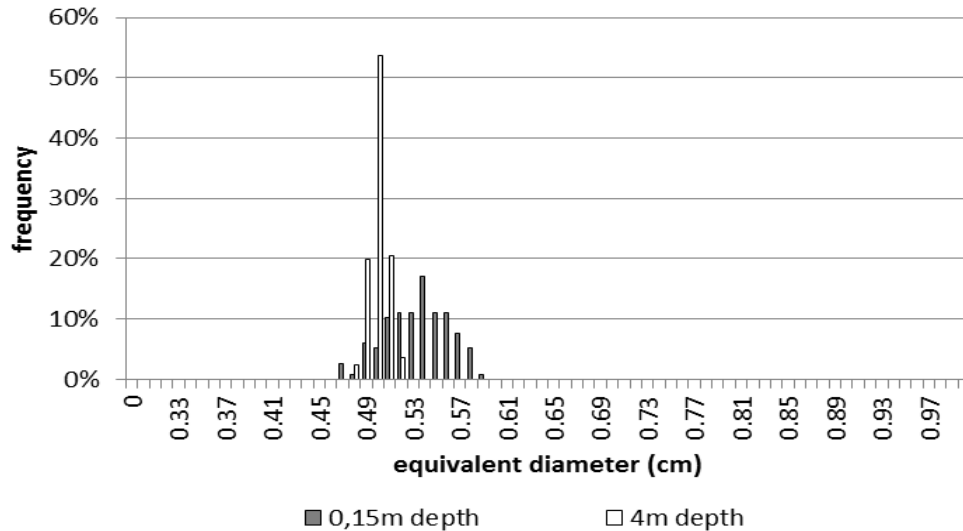

Figure 3. Bubble distribution with a nozzle of 4 mm inside diameter and a nitrogen mass flow rate of 0.033 l/min

4.1.1   Influence of the Injection Flow Rate on Bubble Size and Terminal Velocity

The slip velocity in a bubble plume, i.e. the velocity difference between rising bubbles and the surrounding liquid, is dependent on the bubble size (Zheng and Yapa, 2000). In this way, to be sure to consider only the influence of isolated bubble size on the terminal velocity in stagnant liquid, the first step is to establish the ideal flow rate conditions.

To evaluate the flow rate impact on bubble size and terminal velocity, 7 different flow rates of air were tested between 300 rpm (i.e. 5 mL.min^{-1} in atmospheric pressure conditions) to 3500 rpm (i.e. 60 mL.min^{-1} in atmospheric pressure conditions). Figure 4 shows the terminal velocities and the corresponding equivalent diameter measured for the different flow rate conditions close to the injection outlet (4 m depth) and 3.75 m above it (0.25 m depth). Near the nozzle, when the injection rate (outlet pressure) increases, the bubble size and the associated velocity increase, from 22.8± 1.1 cm.s^{-1} for a bubble equivalent diameter of 4.4 ± 0.1 mm, to a maximum velocity of 28.2 ± 0.7 cm. s^{-1} for an equivalent diameter of 5.0 ± 0.4 mm. Higher up in the water column, 3.75m above the injection outlet, a slight increase in the equivalent diameter and the terminal velocity is observed when the flow rate increases to a peak reached at 2350 rpm. At this flow rate, the maximum terminal velocity is 26.9 ± 1.8 cm.s^{-1} for an equivalent bubble diameter of 5.4 ± 0.3 mm. The decrease in the velocity observed after this point may be explained by the distance between the bubbles during the ascension. The distance between the rising bubbles is known to affect their terminal velocity (Castillejos and Brimacombe, 1987).
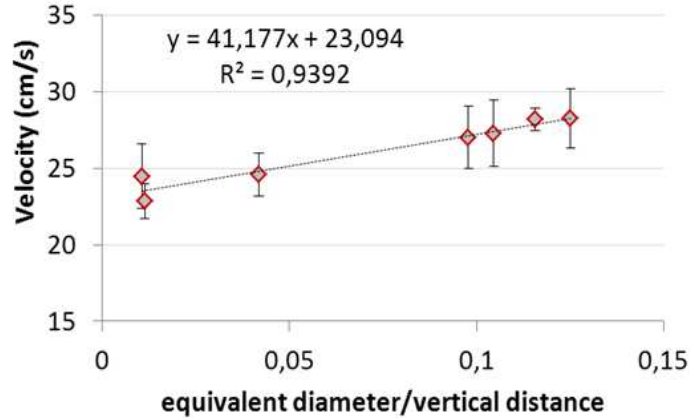
Parthenay, V., Y.-H. Hellouvry, A. Laurent, S. Le Floch, S. Van Ganse, G. Blanchetière and M. Mouriès, METANE: An Integrated Project to Model Underwater Gas/Oil Blowouts and LNG Leaks, Proceedings of the Thirty-seventh AMOP Technical Seminar on Environmental Contamination and Response, Environment Canada, Ottawa, ON, pp. 102-121, 2014.

Figure 4. Influence of the ratio equivalent diameter/vertical distance on the terminal velocity (cm/s) of the bubbles.

The results of the influence of the distance separating bubbles on their velocity are presented in Figure 4. These results are obtained close to the injection nozzle. It was not technically possible to produce the same analysis 3.75 m above it. During their ascension, the bubbles may separate on the horizontal plane and are therefore not visible on the recorded images.

The linear correlation between the increase in the terminal velocity and the increase in the "equivalent diameter/vertical distance" ratio is shown on the graph. This graph does not clearly show the intermediate stage between the momentum-motion and the buoyant-motion, at which terminal bubble velocities are not affected by the turbulence fields from the other bubble. This promising result needs to be studied in further experiments in order to determine the buoyant velocity in numerical models predicting the rise of the gas to the surface depending on the bubble size and also the distances between bubbles.

4.1.2 Bubble Terminal Velocity

In this experiment, the influence of the diameter of the gas bubble has been described for nitrogen gas and air. To be sure that the flow rate does not affect the measurement, the minimal distance between two bubbles is 40 cm (equivalent diameter/vertical distance ratio lower than 0.01). Figure 5 shows experimental data on nitrogen bubbles with different terminal velocity regimes depending on the bubble equivalent diameter. The first part of the curve describes the velocity of spherical shape bubbles. In the second part of the curve, the bubbles are characterised by an ellipsoidal shape and the terminal velocity follows a new equation. For the nitrogen gas, the diameter between spherical and ellipsoidal regimes observed (critical diameter) is 1.5 mm. Comparison of Clift's equation and the experimental data shows strong correlation. In the same way, Figure 6 and Figure 7 present preliminary results respectively for nitrogen and air bubble velocity. The correlation between the experimental data and Clift's equation confirms consistency with Clift's formulation.
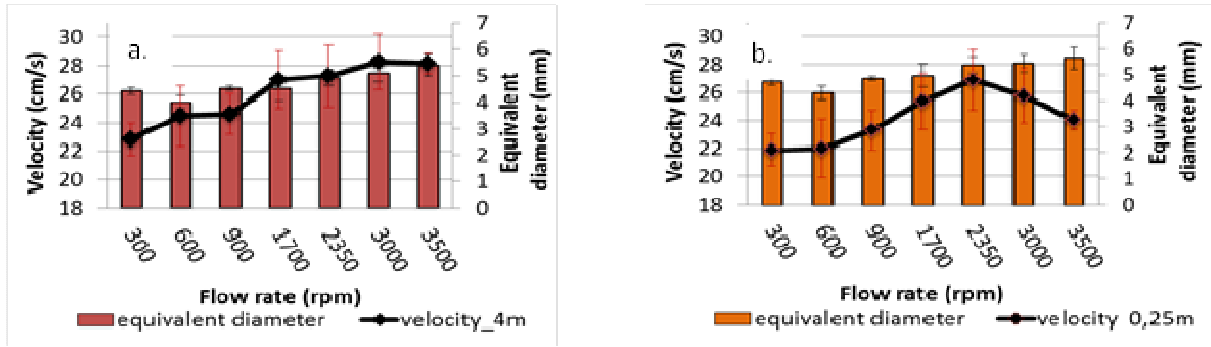
Parthenay, V., Y.-H. Hellouvry, A. Laurent, S. Le Floch, S. Van Ganse, G. Blanchetière and M. Mouriès, METANE: An Integrated Project to Model Underwater Gas/Oil Blowouts and LNG Leaks, Proceedings of the Thirty-seventh AMOP Technical Seminar on Environmental Contamination and Response, Environment Canada, Ottawa, ON, pp. 102-121, 2014.

Figure 5. Terminal velocity (cm/s) and equivalent diameter (mm) of the bubbles measured at 4 m depth (a) and 0.25 cm depth (b).
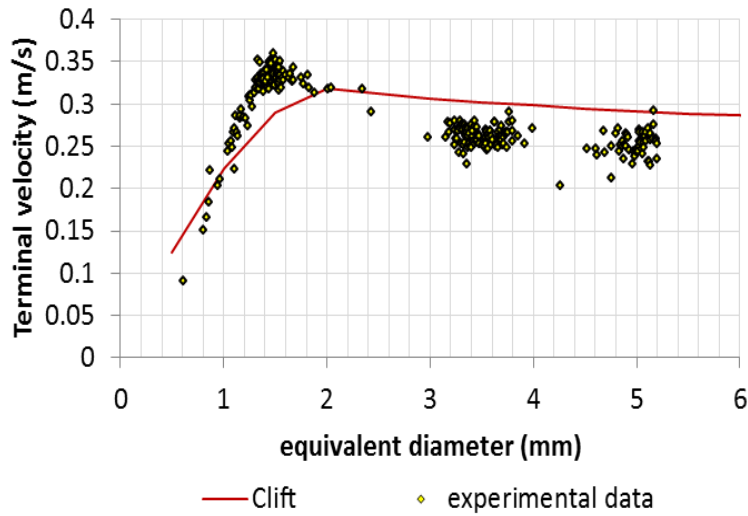

Figure 6. Terminal velocity (m/s) of nitrogen in seawater at 10°C and Clift's correlation.
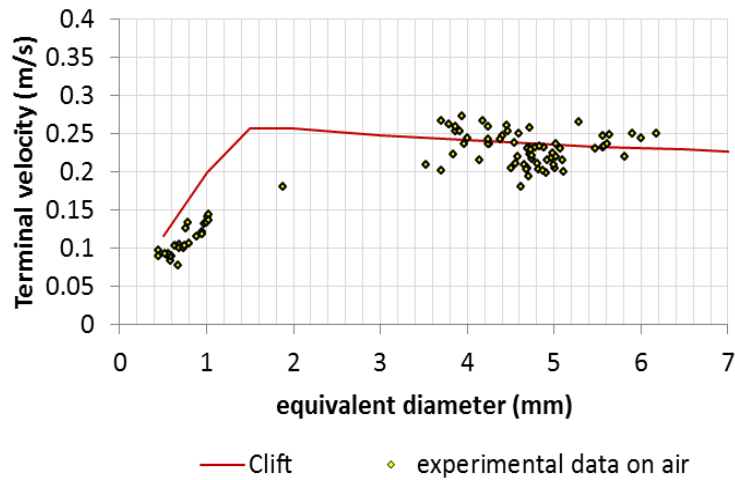

Figure 7. Terminal velocity (m/s) of air bubbles in seawater at 10°C and Clift's correlation (interfacial tension: 0.0139N.m⁻¹)

Parthenay, V., Y.-H. Hellouvry, A. Laurent, S. Le Floch, S. Van Ganse, G. Blanchetière and M. Mouriès, METANE: An Integrated Project to Model Underwater Gas/Oil Blowouts and LNG Leaks, Proceedings of the Thirty-seventh AMOP Technical Seminar on Environmental Contamination and Response, Environment Canada, Ottawa, ON, pp. 102-121, 2014.

4.2   High pressure experiments

To investigate the influence of pressure on the bubble behaviour, experiments were performed in a pressurized vessel able to simulate high depth release down to 800 m (80 bar). This device presents an inside diameter of 6 inches for a total height of 1.70 m. Twenty vertical glass windows are arranged above the 360° position to observe the development of the bubble flow from the injection point to the top of the column. The nozzle is located at the first glass window level and presents an inside diameter of 1 mm. A static pressure sensor and a thermocouple (type K) are located on the gas injection system to respectively control the pressure and the temperature inside the column during experimental tests.
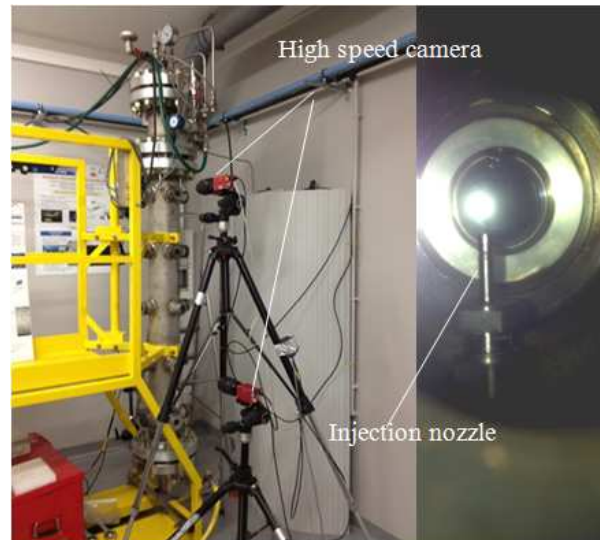
Figure 8. Picture of the atmospheric vessel with high speed camera position and location of the gas injection nozzle.

Tests were performed with nitrogen and methane in a range of pressure between 1 and 80 bar. Video measurements were performed using an optical technique called shadowgraphy. This technique is based on back light illumination of the pressurized column by a collimated light combined with a high speed camera (Figure 8). Two video cameras were used for these tests, one located at the second level of glass windows, and the other one at the top level of glass windows. The distance between the two cameras is 90 cm and the bottom camera was located 30 cm from the injection nozzle. For each operating pressure, three tests were performed with a video acquisition time of 30s. The region of interest for the cameras is almost 3.5 cm.

The equivalent bubble diameter is based on the Waddle diameter. Figure 9 presents the influence of the pressure on the mean equivalent diameter for nitrogen and methane experiments. This figure shows a decrease in the mean bubble diameter as the pressure increases. This variation corresponds to a 38% decrease in bubble diameter for nitrogen and a 27% decrease for methane between atmospheric and 80 bar pressure tests. This result was also obtained in the literature by several authors (Lin et al. 1998 and Li et al., 2000) and confirms, as an initial approach, the ideal gas law which describes the decrease in bubble volume as the surrounding pressure increases.
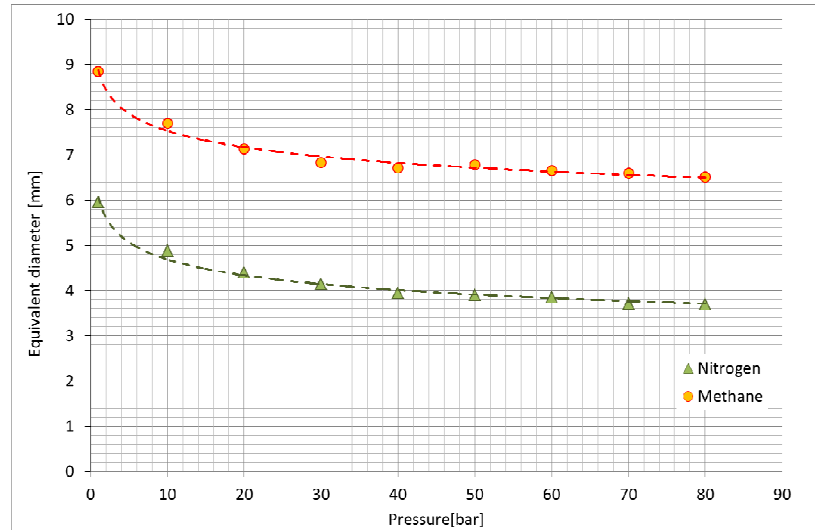
Figure 9. Characterisation of operating pressure influence on bubble equivalent diameter for nitrogen and methane experiments

Bubble velocity is an important parameter to determine plume flowing time and the area impacted by the blowout at the sea surface. The evaluation of this parameter is imperative and requires good accuracy. Based on the objectives, the bubble velocity was evaluated experimentally for each pressure using the position of the bubble mass center on each picture, the pixel resolution and the camera frame rate. A maximum of 200 pictures were analyzed for each pressure, all the non-entire bubbles were rejected and a minimum of two consecutive images with the same bubble was required to determine the velocity.

All experimental data were compared with the velocity formulation proposed by Clift (1978). The previous analysis revealed that many bubbles present ellipsoidal shape and based on this assumption the velocity formulation for the ellipsoidal shape regime was used (equation 7). Figure 10 presents a comparison between experimental data performed with methane for bubble gas velocity and Clift's model. The Figure clearly shows that 100% of data are predicted in a range of 20%. It demonstrates that there are uncertainties on fluid physical parameters when operating conditions are up to 46 bars which is the critical pressure of Methane. Beyond this value, the fluid is in a supercritical state and fluid physical data are difficult to estimate.
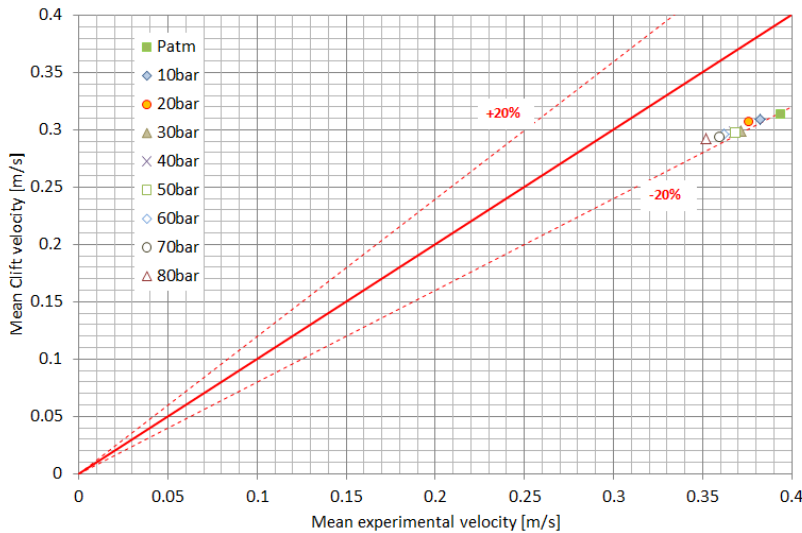
Figure 10. Comparison of mean velocity obtained with Clift's theory and mean experimental data obtained with methane

5.   Coupling BLOWOUT with atmospheric dispersion/fire models

BLOWOUT's results were coupled with atmospheric dispersion (as represented on Figure 11) and fire modelling tools for selected accidental scenarios to perform a first comprehensive risk evaluation. Best practices have also been highlighted to model such configurations.
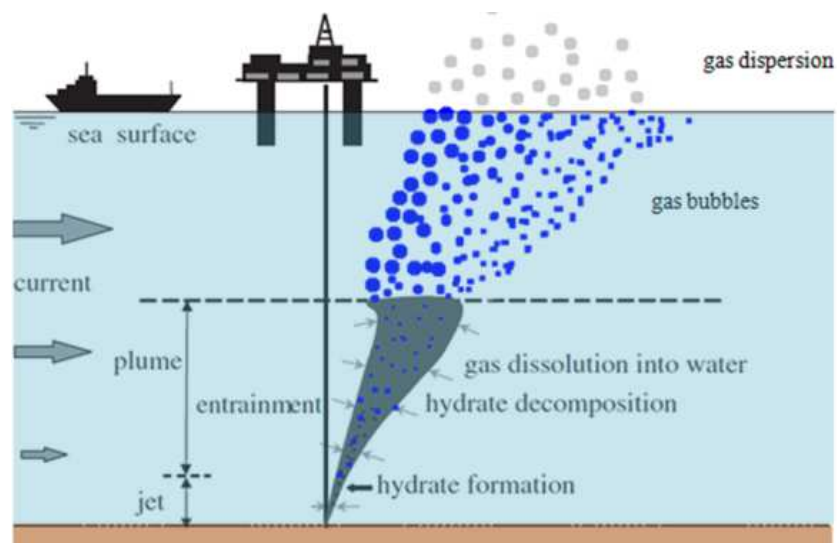
Figure 11. BLOWOUT results defining gas reaching the sea surface are used for flame and dispersion modeling

Scenarios involving a 50 mm diameter puncture at several water depths (~ 20 and 100 meters) have been studied. The direction of the 50 mm diameter puncture (vertical or horizontal) mainly impacts the location where the plume will reach the water surface without changing gas source term characteristics (plume velocity, radius and void fraction).

The rupture scenario (mass flow ~ 1000 kg.s^{-1}) was not retained for atmospheric dispersion study. The gas velocity at the sea surface, calculated by BLOWOUT around 10

Parthenay, V., Y.-H. Hellouvry, A. Laurent, S. Le Floch, S. Van Ganse, G. Blanchetière and M. Mouriès, METANE: An Integrated Project to Model Underwater Gas/Oil Blowouts and LNG Leaks, Proceedings of the Thirty-seventh AMOP Technical Seminar on Environmental Contamination and Response, Environment Canada, Ottawa, ON, pp. 102-121, 2014.

m.s^{-1}, indeed leads to high water level elevation (estimated up to 5-10 m) that cannot be correctly integrated in dispersion/fire models where the sea surface has to be considered flat.

Two different softwares are used to achieve the atmospheric dispersion calculations:
- KAMELEON software (KFX): A "Computational Fluid Dynamics" tool - RANS model of k-ε standard type
- PHAST software: A "simple" model - Gaussian and integral

For flame and dispersion simulation, Neutral "D" and Stable "F" Pasquill classes were studied because they lead to higher flammable clouds compared to unstable wind conditions where the higher turbulence reduces the size of the plume. The range of the flame and dispersion results obtained with KFX are presented in the Table 1:

50 mm leak diameter scenario – KFX results range	
Flammable cloud maximal size [m]	
Cloud length	60 - 105
Cloud height	5 - 20
Flame maximal size and radiation distance [m]	
Flame length	15 – 30
Flame height	

Table 1. KFX results
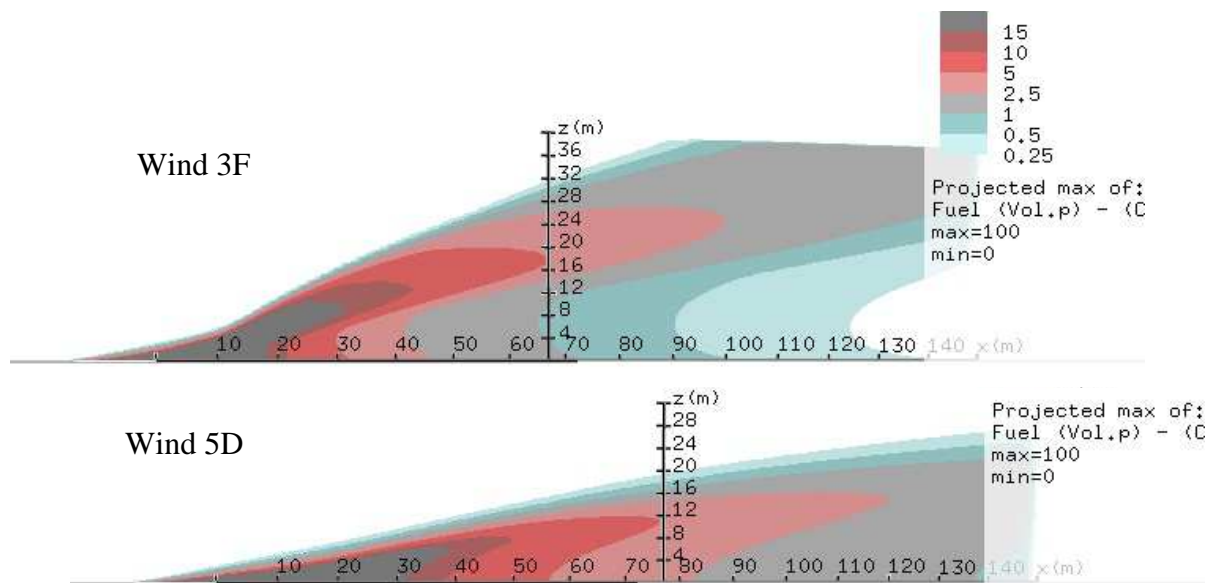
Figure 12. 50 mm diameter leak on pipe located at a 100 meters water depth – Projected view (XoZ) of the flammable cloud (in dark red) in the atmosphere get with KFX

This study also showed that no method with an existing "simple" model from PHAST software gives acceptable results (compared to CFD results). Specific source term development is thus needed before using a "simple" standard gas dispersion model. In the meantime, it is advised to preferably use CFD (as KFX software) to couple with results from BLOWOUT.

6. Presentation of METANE Tool

The METANE tool is made up of a computing code which is reachable through a graphical user interface (GUI) providing access to the initialization of the computation process and to the post-treatment and visualization of the results (Figure 13). Scenario definition is set in specified tabs.

The oil/natural gas tab is organized into several group boxes gathering parameters:

- Simulation options: The user can decide on the type of pollutant i.e. oil, gas, or oil and natural gas release, and select the modules he wants to activate, such as automatic entrainment coefficient, gas dissolution, etc. A batch mode is also available to perform a parametric study on the break size or the flow rate of the leak.
- Break parameters: This gathers all the release characteristics such as break diameter, the oil/gas volumetric flow rate, break location and orientation, temperature of the pollutant and initial bubble size (if gas is present).
- Ambient parameters: The user can provide fixed values or data profiles for the ambient environment for the temperature, salinity and current.
- Advanced parameters: As an expert mode, this allows tuning variables to be changed from the used models, such as entrainment coefficient, or physical and chemical constants for the oil/gas/water entities.

For LNG releases, the simulation parameters are also organized into group boxes: Release configuration, release parameters, environmental parameters (water column and atmospheric), properties of LNG droplets and vapour bubbles.
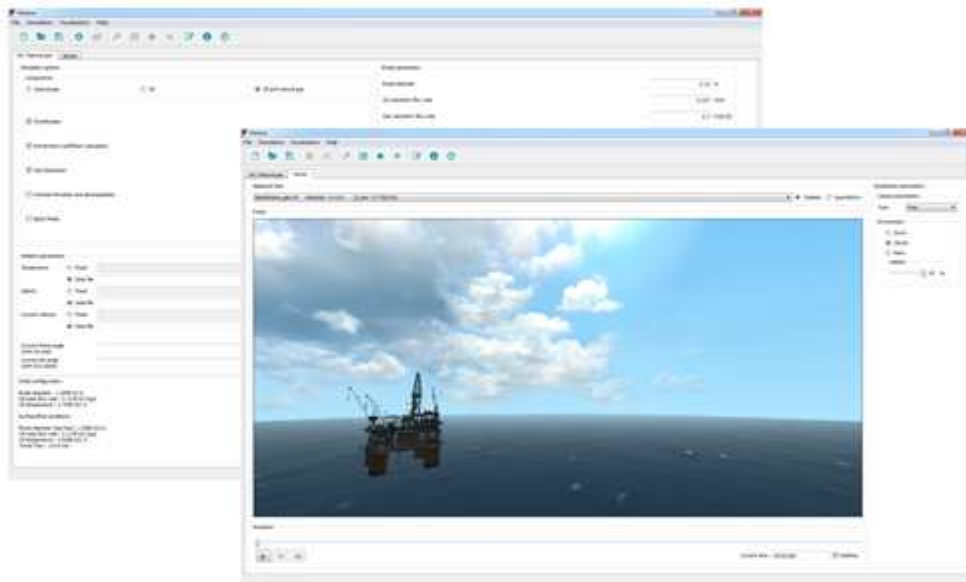
Figure 13. METANE tool GUI, oil/natural gas configuration tab and viewer tab

The viewer tab contains the 3D visualization (Figure 13), where the user can freely move around the scene. It also contains the view mode (realistic or quantitative view), view options (such as weather types), and the video recorder to play the chosen scenario and animate the plume rising.

The scene render was developed with Renderbox, an Alyotech dedicated 3D simulation engine, and with a OpenSceneGraph multiplatform 3D engine based on OpenGL. Major efforts have been made to give a realistic visualization of the subsea environment and plume (Figure 14, Figure 15 and Figure 16):

- Visibility attenuation with depth, tuning turbidity, and particles in suspension. A ROV spotlight can be activated.
- Surface ray light refraction, "god-rays", animated with the surface waves and light variation with the weather.
- Adaptative and realistic topology of the seafloor depending on the depth of release. Presence of subsea vegetation.

Surface interaction is also considered (Figure 17), such as an oil slick with a representative drift due to current, or the "boiling" fountain for gas release.
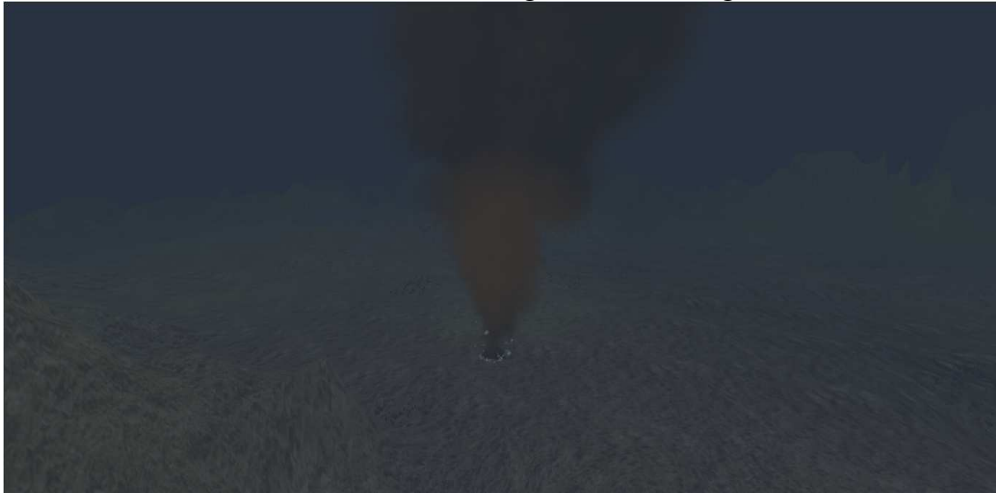

Figure 14. Oil release example: Realistic environment and ROV light effects

Figure 15. Natural gas release example: Realistic environment and ROV light effects
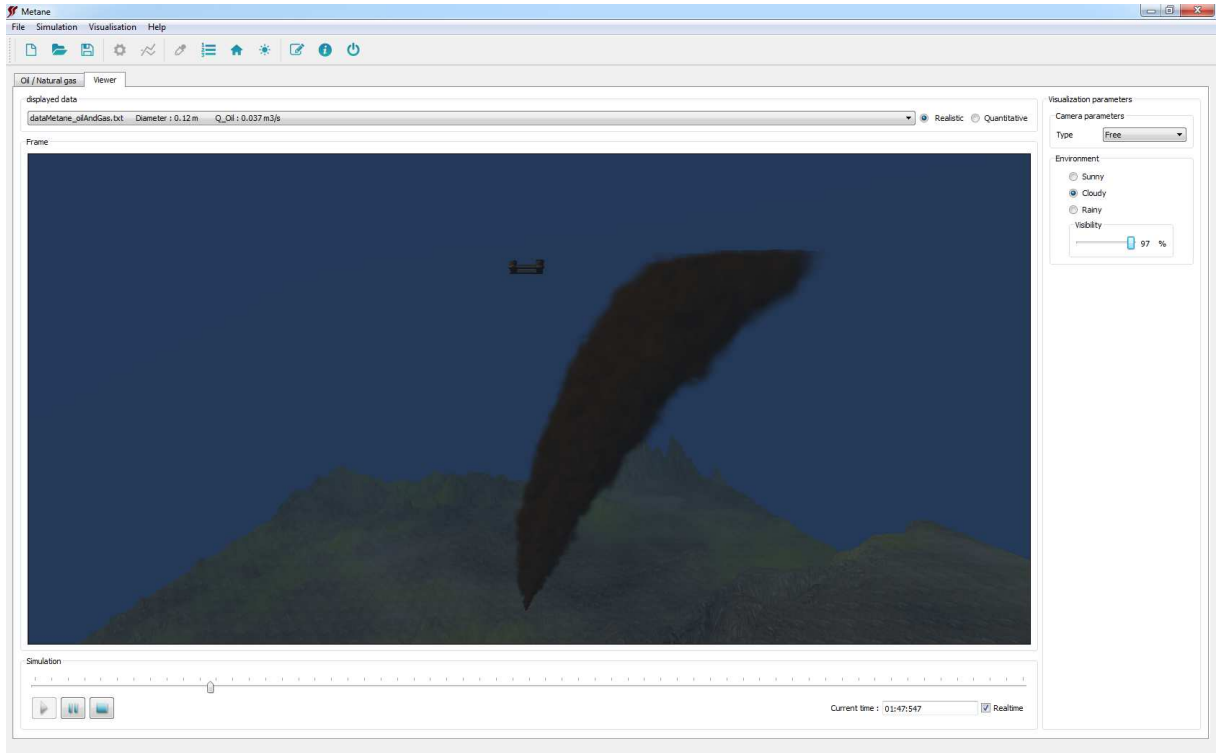
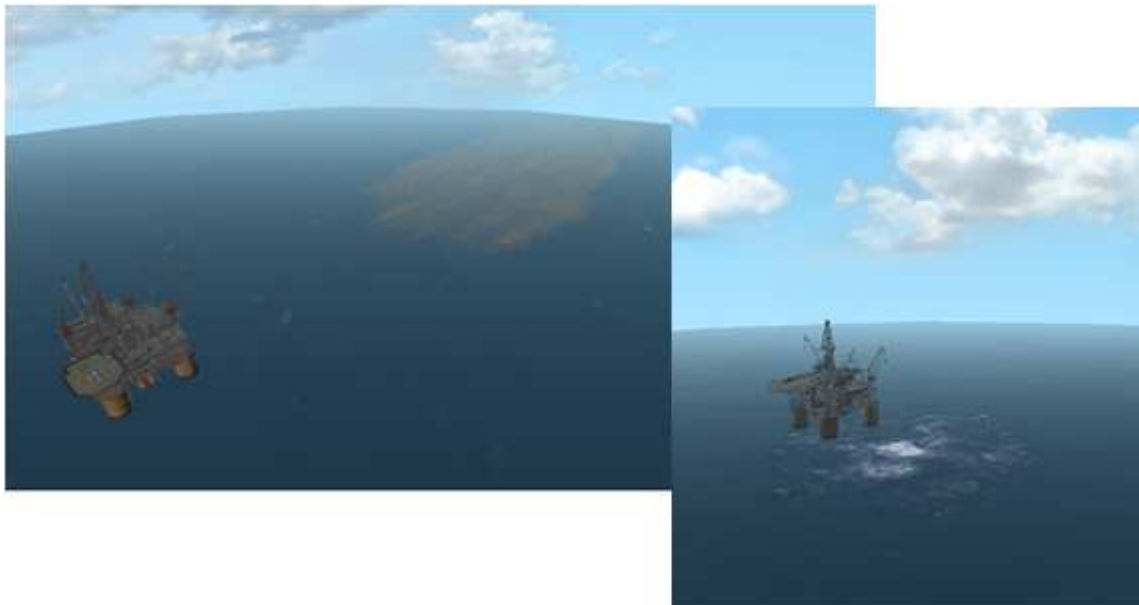**Figure 16. Oil release example: General view of the subsea plume**

Figure 17. Oil release example: Surface oil slick and natural gas release example: Surface boiling fountain

Results from the simulation are directly exploitable in the quantitative view: displaying plume slices or a cut view, picking points in the plume to obtain information about oil/natural gas concentration, velocity, etc. (Figure 18). 2D plot outputs are also available, giving extra information on surface pollutant concentration, or fountain elevation with radius (Figure 19). For LNG release simulation, 2D plot outputs provide information on

Parthenay, V., Y.-H. Hellouvry, A. Laurent, S. Le Floch, S. Van Ganse, G. Blanchetière and M. Mouriès, METANE: An Integrated Project to Model Underwater Gas/Oil Blowouts and LNG Leaks, Proceedings of the Thirty-seventh AMOP Technical Seminar on Environmental Contamination and Response, Environment Canada, Ottawa, ON, pp. 102-121, 2014.

droplet/vapour bubble temperature when reaching the surface (Figure 20), as well as concentration and mass flow rate values with radius.

These results have been validated by comparisons with:

- Experiments (made by CEDRE, EMA during METANE's project and BLOWOUT's project and made by OCEANIDE during BLOWOUT's project),
- CFD simulations (made by DORIS during BLOWOUT's project).
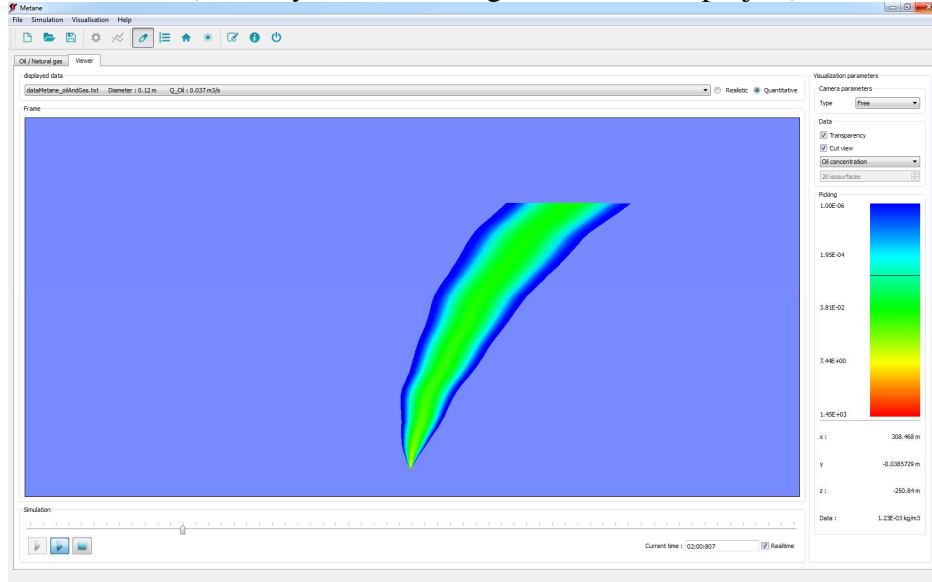
Figure 18. Quantitative view of the plume and concentration picking
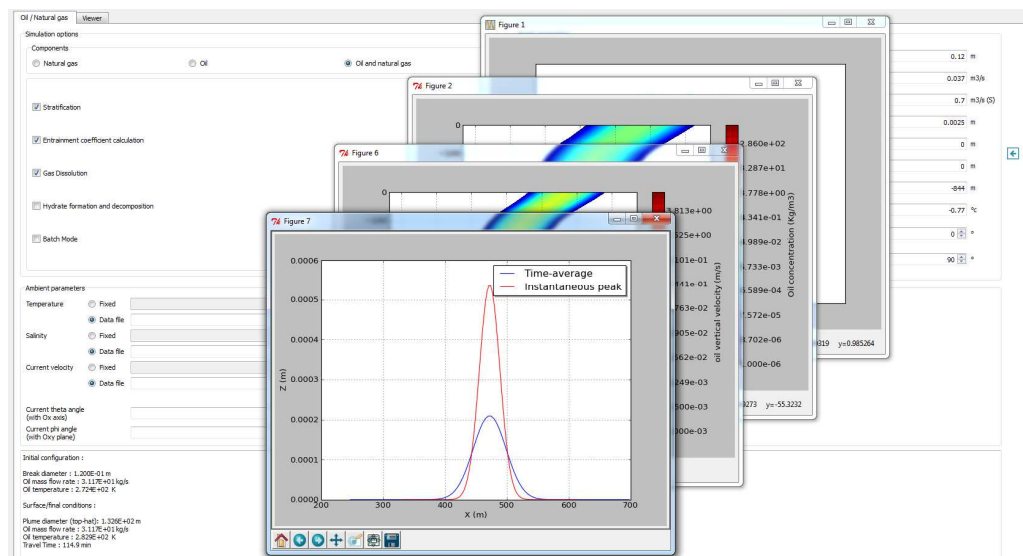
Figure 19. Oil/natural gas 2D plots

Parthenay, V., Y.-H. Hellouvry, A. Laurent, S. Le Floch, S. Van Ganse, G. Blanchetière and M. Mouriès, METANE: An Integrated Project to Model Underwater Gas/Oil Blowouts and LNG Leaks, Proceedings of the Thirty-seventh AMOP Technical Seminar on Environmental Contamination and Response, Environment Canada, Ottawa, ON, pp. 102-121, 2014.
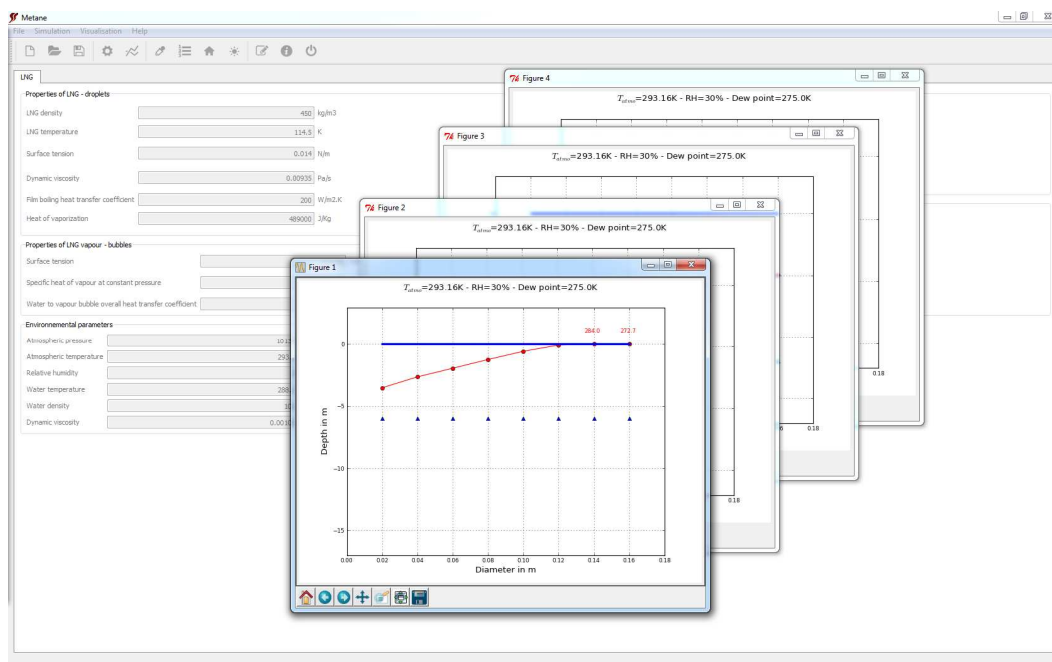
Figure 20. LNG plot results

7. Acknowledgements

8. References

Castillejos, A.H. and J.K. Brimacombre, "Measurement of Physical Characteristics of Bubbles in Gas_Liquid Plumes: PartII. Local Properties of Turbulent Air-Water Plumes in Vertically Injected Jets". *Metall Trans B*, 18:659-671, 1987.

Clift R., J.R. Grace, M.E. Weber, "Bubbles, Drops and Particles", *Academic Press*, New York, 1978.

Englezos P., N. Kalogerakis, P.D. Dholabhai, P.R. Bishnoi, "Kinetics of Formation of Methane and Ethane Gas Hydrates", *Chemical Engineering Science*, Vol.42, No. 11, pp. 2647-2658, 1987.

Lee J. H. W.; V. Cheung, "Generalized Lagrangian Model for Buoyant Jets in Current", *Journal of Environmental Engineering*, Vol.116, 1990.

Le Floch, S., H. Benbouzid, Olier, R., "Operational Device and Procedure to Test the Initial Dissolution Rate of Chemicals After Ship Accidents: the Cedre Experimental Column", *The Open Environmental Pollution & Toxicology Journal*, 1: 1-10, 2009.

Li Y., J. Zhang, L.-S. Fan, "Discrete-Phase Simulation of Single Bubble Rise Behaviour at Elevated Pressure in a Bubble Column", *Chemical Engineering Science*, Vol. 55, pp. 4597-4609, 2000.